Journal of Power Sources 183 (2008) 609–618

Contents lists available at ScienceDirect

Journal of Power Sources

journal homepage: www.elsevier.com/locate/jpowsour

Two-phase modeling of gas purge in a polymer electrolyte fuel cell

Puneet K. Sinha[1], Chao-Yang Wang*

Electrochemical Engine Center (ECEC), Department of Mechanical and Nuclear Engineering, The Pennsylvania State University, University Park, PA 16802, United States

ARTICLE INFO

Article history:
Received 30 April 2008
Received in revised form 28 May 2008
Accepted 29 May 2008
Available online 7 June 2008

Keywords:
Gas purge
GDL drying
Membrane drying
Experimental validation
Polymer electrolyte fuel cell

ABSTRACT

Gas purge intended to minimize residual water in a polymer electrolyte fuel cell (PEFC) is critical for successful shutdown and sub-zero startup. In the present work, we present a two-phase transient model describing water removal from PEFC under gas purge conditions. The role of back diffusion from the cathode to anode along with liquid water transport in the gas diffusion layers behind the drying front and vapor diffusion ahead of the drying front is highlighted. The underlying ineffectiveness of cathode-only purge is outlined. The model predictions are compared with experimental results under various purge conditions. A good match with experiments is obtained at higher purge temperatures whereas some differences in the HFR profile is observed at lower temperatures. The role of drying front morphology in addressing the observed differences between numerical and experimental results is hypothesized.

1. Introduction

In recent years, rapid startup of a polymer electrolyte fuel cell (PEFC) from sub-zero temperatures, more commonly known as cold start, has emerged as one of the key challenges in realizing PEFC technology for automotive applications. Various studies delineating the fundamental mechanism of cold start have been published [1–6]. It is recognized that product water becomes ice upon startup when the cell temperature is below the freezing point of water. The product water created in a sub-zero environment may diffuse into the membrane if it is dry initially, or otherwise precipitates as ice or frost in the cathode catalyst layer (CL), leading to CL plugging by solid water and PEFC shutdown before the cell temperature rises above freezing. It thus follows that a drier membrane prior to cold start facilitates longer operation time during cold start. Typically gas purge is performed for control and minimization of residual water in a PEFC prior to engine shutdown. Therefore, detailed understanding of gas purge is essential to establish effective gas purge protocols to aid successful cold start of PEFC. In this context, an effective purge can be defined as the one that provides a certain high value of the membrane high-frequency resistance (HFR) in the shortest amount of time, noting that membrane HFR is a direct measure of membrane hydration.

Water removal from PEFC during gas purge can be viewed as a process similar to convective drying of a porous medium. In the past, various macroscopic models have been proposed to investigate convective drying of hydrophilic porous media for applications ranging from soil science to food processing. These models have either adopted Luikov's phenomenological approach [7] using thermodynamics theory of irreversible processes to describe the temperature, moisture and pressure distributions in a porous medium during drying, or Whitaker's volume averaging method [8]. The majority of published models [9–14] follow Whitaker's approach, and thus treat convective drying as a classical problem of coupled heat and mass transfer in porous media. At the macro-scale drying is further divided into funicular stage in which liquid transport due to capillary flow is dominant and pendular stage where moisture movement is solely driven by vapor diffusion. Funicular and pendular stages are distinguished at the onset of irreducible liquid saturation in several macroscopic models [15,16]. Two-phase Darcy's law is generally used to investigate funicular stage, whereas over the years several modifications have been proposed to address liquid phase removal in pendular stage: liquid phase removal due to evaporation only [17], incorporation of liquid transport through liquid films along the corners [18] and mass transfer due to chemical potential gradient [19], to name a few. In contrast, drying of a hydrophobic porous medium has been scarcely researched. Most recently, Shahidzadeh-Bonn et al. [20] experimentally investigated the effect of wetting properties on drying and showed substantial differences in drying rates of hydrophilic and hydrophobic porous media. This investigation confirmed the absence of constant rate period, an important characteristic of hydrophilic porous medium drying, during drying of a hydrophobic porous medium. Tajiri et al.

* Corresponding author. Tel.: +1 814 863 4762; fax: +1 814 863 4848.
E-mail address: cxw31@psu.edu (C.-Y. Wang).
[1] Present address: GM Global Research and Development, General Motors Fuel Cell Activities, Honeoye Falls, NY 14472, United States.

0378-7753/$ – see front matter © 2008 Elsevier B.V. All rights reserved.
doi:10.1016/j.jpowsour.2008.05.078

Nomenclature

a	water activity
A	area (m^2)
C_k	molar concentration of species k ($mol\,m^{-3}$)
D_w^g	diffusivity of water vapor ($m^2\,s^{-1}$)
D_w^m	membrane water diffusivity ($m^2\,s^{-1}$)
EW	equivalent weight of membrane
k_r	relative permeability
K	absolute permeability (m^2)
m_w	mass fraction of water
M_w	molecular weight of water ($kg\,mol^{-1}$)
n	Brugemann factor
P	pressure (Pa)
P_c	capillary pressure (Pa)
Q	purge gas flow rate ($m^3\,s^{-1}$)
R	gas constant ($8.314\,J\,(mol\,K)^{-1}$)
s	liquid water saturation
t	time (s)
T	temperature (K)
$\vec{u}$	velocity vector ($m\,s^{-1}$)
V	volume (m^3)

Greek letters

ε	porosity
θ	contact angle
λ	membrane water content
λ_k	mobility of phase k
ν	kinematic viscosity
ρ	density ($kg\,m^{-3}$)
σ	surface tension ($N\,m^{-1}$)

Superscripts and subscripts

eff	effective
g	gas phase
l	liquid phase
m	membrane phase
o	standard condition, 273.15 K, 1.013 kPa (1 atm)
sat	saturate value

[21] developed an experimental method for gas purge in a PEFC for the first time and presented purge curves under a wide range of operating conditions.

Gas purge though analogous to convective drying of a porous medium requires exhaustive investigations to delineate the underlying mechanisms. The need originates from the hydrophobic nature of gas diffusion layer (GDL), thin layers of GDL (~200 μm), CL (~10 μm) and membrane (10–50 μm), presence of current-collecting lands obstructing water removal, and the presence of ionomer in CL and membrane. Bradean et al. [22] showed, based on a one-dimensional (1D) purge model, that the cell temperature is the most sensitive parameter controlling purge effectiveness. However, no efforts were made to explain the underlying physics. Ge and Wang [6] measured the membrane HFR as a function of purge time and correlated HFR increase with the presence of liquid water in CL and GDL. Sinha et al. [23] measured liquid water removal from GDL by purge gas using X-ray microtomography. They showed that purge gas erodes liquid water clusters in the GDL, giving birth to small isolated clusters that can be removed only by evaporation, resulting in exponential decay in drying rate. Most recently, Sinha and Wang [24] presented an analytical purge model describing GDL and membrane drying during gas purge. Although this model sheds fundamental insight into gas purge phenomena, it ignores liquid water transport behind the drying front and simplifies the treatment of ionomer dehydration. Additionally, the model is for the cathode only, thus neglects any water transport between the cathode and anode sides through the membrane. These simplifying assumptions limit the applicability of the analytical model in elucidating complex processes of gas purge under realistic conditions. In this article, we present a fully two-phase, multi-dimensional, transient gas purge model with exhaustive treatment of GDL and ionomer drying. The article is organized as follows: first, a detailed description of the governing equations of gas purge is presented. Subsequently, the role of capillary transport of liquid water, vapor diffusion, and interaction between anode and cathode sides in water removal during gas purge is discussed in detail. Finally, the model predictions are compared with gas purge experiments.

2. Numerical model

The present three-dimensional two-phase transient gas purge model is developed based on the previous work of Wang and Wang [25] and Luo et al. [26]. Computational domain of the present model consists of all the regions of a PEFC: gas channels, gas diffusion layers, catalyst layers, bipolar plates on both anode and cathode side, and the ionomeric membrane. The following assumptions are made in the present model:

(I) ideal and incompressible gas mixtures;
(II) laminar flow due to small flow velocities;
(III) isotropic and homogeneous porous layers, characterized by an effective porosity and a permeability;
(IV) isothermal due to large thermal mass of PEFC materials.

With the above assumptions, gas purge is governed by conservation of mass, momentum and species summarized in Table 1. The important species involved in gas purge are purge gas and water. Hence, the species equation is solved only for water. Here, the two-phase mixture density, velocity and viscosity are given by [27]:

$$\rho = \rho^l \cdot s + \rho^g \cdot (1 - s) \tag{1}$$

$$\rho\vec{u} = \rho^l \cdot \vec{u}^l + \rho^g\vec{u}^g \tag{2}$$

Here, s and $(1 - s)$ denote the volume fraction of the open pore space occupied by liquid and gas phases, respectively. The liquid water saturation, s, can be expressed as a function of mixture water mass fraction, m_w:

$$s = \frac{V^l}{V_{pore}} = \frac{\rho m_w - C^g_{w,sat}M_w}{\rho^l - C^g_{w,sat}M_w} = \frac{\rho^g m_w - C^g_{w,sat}M_w}{\rho^l(1 - m_w) + \rho^g m_w - C^g_{w,sat}M_w} \tag{3}$$

The momentum equation is modified to be valid both in the open channel and the porous layers, i.e. GDL and CL, reducing to the two-phase Darcy's law within the porous layers with a small permeability. Inside the flow channel, porosity and permeability are set to be unity and infinity, respectively. Since the available pore space in the porous GDL and CL is shared by gas and liquid phases, a

Table 1
Two-phase, transient purge model: governing equations

	Governing equations
Mass	$\frac{\partial(\varepsilon\rho)}{\partial t} + \nabla\cdot(\rho\vec{u}) = 0$
Momentum	Flow channels (N–S Eqs.): $\left[\frac{\partial(\rho\vec{u})}{\partial t} + \nabla\cdot(\rho\vec{u}\vec{u})\right] = -\nabla p + \nabla\cdot\tau$ Porous layers (Darcy's Eqs.): $\frac{\mu}{K}\vec{u} = -\nabla p$
Water	$\frac{\partial(\varepsilon\rho m_w)}{\partial t} + \nabla\cdot(\gamma_w\rho m_w\vec{u}) = \nabla\cdot[D_{cap}\,\nabla(m_w)] + \nabla\cdot[\rho^g D_w^{g,eff}\,\nabla(m_w^g)]$

Table 2
Membrane transport properties

Quantity	Value	Reference
Membrane water uptake (λ)	$\lambda = [1 + 0.008a^2(T - 303.15)](14a^3 - 19a^2 + 13a) \quad s = 0$ $\lambda = 0.18(T - 273.15) + 9.2 \quad s > 0$	Assumed
Membrane water diffusivity	$D_w^m =$ for $\begin{cases} 2.692661843 \times 10^{-6} & \text{for } \lambda \le 2 \\ [0.87(3-\lambda) + 2.95(\lambda - 2)] \times 10^{-10} e^{(7.9728-(2416/T))} & \text{for } 2 < \lambda \le 3 \\ [2.95(4-\lambda) + 1.64245(\lambda - 3)] \times 10^{-10} e^{(7.9728-(2416/T))} & \text{for } 3 < \lambda \le 4 \\ [2.653 - 0.33\lambda + 0.0264\lambda^2 - 0.000671\lambda^3] \times 10^{-10} e^{(7.9728-(2416/T))} & \text{for } 4 < \lambda \le 14 \end{cases}$ Gore membrane $D_w^{m,Gore} = 0.5 D_w^m$	Ju et al. [31]
Proton conductivity (κ)	$\kappa = \exp\left[1455\left(\frac{1}{303} - \frac{1}{T}\right)\right]\begin{pmatrix} 0.067a^3 - 0.09a^2 + 0.068a \\ -0.011 \end{pmatrix}$	Tajiri [32]
Note: water activity at the membrane-GDL interface is calculated by	$a = \frac{C}{C_{sat}}$ if $s = 0$ $a = \frac{s(\rho_l/M^{H_2O}) + (1-s)C_{sat}}{C_{sat}}$ if $s > 0$	Pasaogullari and Wang [33]

relative permeability term, k_r^α, is introduced to represent the ratio of intrinsic permeability of phase α at a given saturation level, s, to the total intrinsic permeability of the porous medium. Therefore, the individual phase flux is expressed by Darcy's law using the concept of relative permeability as follows:

$$\rho^l \vec{u}^l = -\frac{k_r^l K}{\nu^l} \nabla P^l \tag{4}$$

$$\rho^g \vec{u}^g = -\frac{k_r^g K}{\nu^g} \nabla P^g \tag{5}$$

where the relative permeabilities of individual phases are assumed to be proportional to the fourth power of phase saturations, i.e.:

$$k_r^l = s^4; \quad k_r^g = (1-s)^4 \tag{6}$$

In addition, the mixture kinematic viscosity and the mobility of each phase in the multiphase mixture are defined as

$$\upsilon = \left(\frac{k_r^l}{\nu^l} + \frac{k_r^g}{\nu^g}\right)^{-1} \tag{7}$$

$$\lambda^l = \frac{k_r^l}{\nu^l}\nu = \frac{k_r^l/\nu^l}{k_r^l/\nu^l + k_r^g/\nu^g} \qquad \lambda^g = 1 - \lambda^l \tag{8}$$

The diffusive mass flux of liquid phase, $\vec{j}^l$, relative to the whole two-phase mixture is expressed as follows:

$$\vec{j}^l = \rho^l \vec{u}^l - \lambda^l \rho \vec{u} = \frac{K}{\nu}\lambda^l \lambda^g \nabla P_c \tag{9}$$

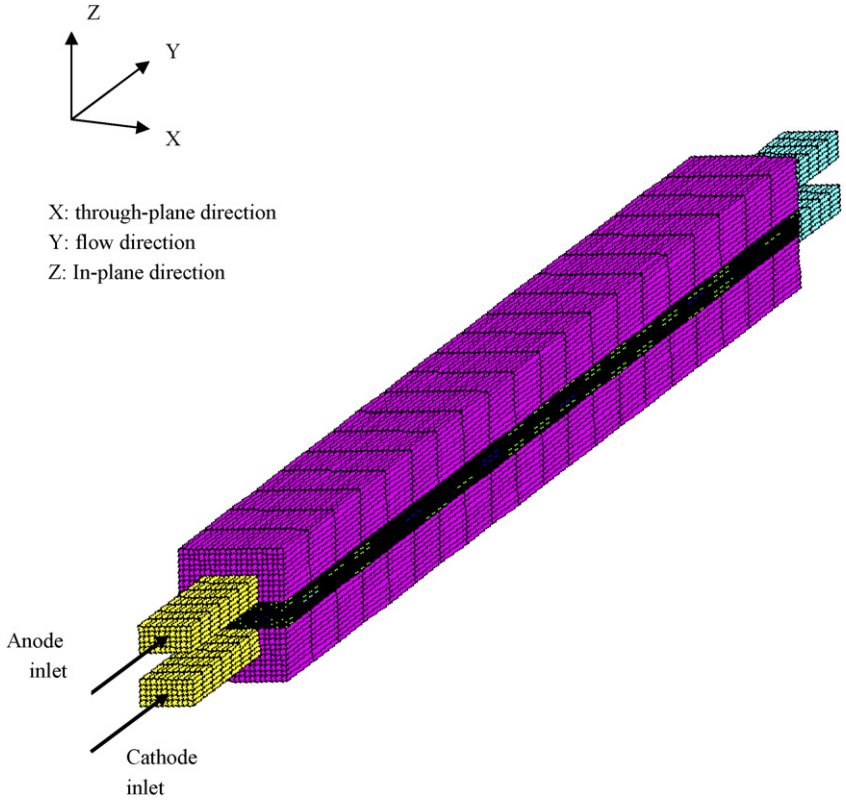

Fig. 1. Cell geometry and mesh configuration.

Table 3
Geometrical parameters and physical properties

Description	Value
Anode/cathode gas diffusion layer thickness	0.230 mm
Anode/cathode catalyst layer thickness	0.010 mm
Anode/cathode gas channel depth	0.5 mm
Anode/cathode gas channel width	1.0 mm
Height of cell in the in-plane direction	2.0 mm
Cell length	54.0 mm
Membrane width (Gore-select®)	0.030 mm
Dry membrane density (ρ_{mem})	2000 kg m^{-3}
Equivalent weight of membrane (EW)	0.95
Porosity of anode/cathode gas diffusion layer (ε_{GDL})	0.6
Porosity of anode/cathode catalyst layer (ε_{cat})	0.6
Bruggemann factor of porous layer for water vapor diffusion (n)	3
Volume fraction of ionomer in anode/cathode catalyst layer (ε_{mc})	0.26
Permeability of anode/cathode gas diffusion layers (K_{GDL})	4.0×10^{-12} m^2
Permeability of anode/cathode catalyst layers (K_{CL})	4.0×10^{-12} m^2
H_2O diffusivity in the gas channels ($D^g_{w,o}$)	2.6×10^{-5} m^2 s^{-1}
Surface tension (σ)	6.25×10^{-2} N m^{-1}
Contact angle (θ)	110°

The capillary pressure, P_c, is defined as

$$P_c = P^g - P^l = \sigma \cos\theta \left(\frac{\varepsilon}{K}\right)^{1/2} J(s) \quad (10)$$

where ε is the porosity and K the permeability of porous layers, θ the contact angle of liquid water in porous layers. The Leverett function, $J(s)$, denotes the dimensionless capillary pressure that is an increasing function of the nonwetting phase saturation (i.e. liquid water saturation in hydrophobic GDL). The Leverett function, $J(s)$ is given as [28]:

$$J(s) = \begin{cases} 1.417(1-s) - 2.120(1-s)^2 + 1.263(1-s)^3 & \text{if } \theta_c < 90^\circ \\ 1.417s - 2.120s^2 + 1.263s^3 & \text{if } \theta_c > 90^\circ \end{cases} \quad (11)$$

In Table 1, the second term on the left-hand side of the water conservation equation represents the advective term, in which the advection correction factor, γ_w is given by:

$$\gamma_w = \frac{\rho(\lambda^l m^l_w + \lambda^g m^g_w)}{(s\rho^l m^l_w + (1-s)\rho^g m^g_w)} = \begin{cases} \dfrac{\rho(\lambda^l + \lambda^g (C_{sat} M_w/\rho^g))}{(s\rho^l + (1-s)C_{sat}M_w)} \end{cases} \quad (12)$$

Therefore, total water is advected by a modified velocity, $\gamma_w \vec{u}$, rather than the original mixture velocity, $\vec{u}$. The first term on the right-hand side for water conservation equation shows the transport of water due to the relative motion between the phases, namely capillary transport that is proportional to the gradient in liquid saturation.

The second term on the right-hand side of the water conservation equation represents the net Fickian diffusion fluxes within gas phase. The gas phase diffusion coefficient of water, D^g_w, in anode and cathode gas channels is calculated as a function of pressure and temperature [29]. For GDL and CL, the diffusion coefficient is modified to account for porosity and tortuosity of porous regions, and is given by:

$$D^g_w = D^g_{w,o}\left(\frac{T}{T_o}\right)^{3/2}\left(\frac{P}{P_o}\right) \quad \text{for gas channel}$$

$$D^{g,eff}_w = \varepsilon^n D^g_w \quad \text{for porous layers} \quad (15)$$

where ε and n are the porosity and Bruggemann factor of porous layers, respectively.

The transient term given by the first term on left-hand side of water conservation equation expresses the removal of liquid water modified to account for the porosity of GDL and CL. It should be mentioned that the diffusive flux, depicted by the second term

Table 4
Pre-purge and base case purge conditions

Parameter	Value
Pre-purge operation	
Inlet RH (anode/cathode)	100%/100%
Stoichiometry (anode/cathode)	18.0/21.0
Flow configuration	Co-flow
Operating temperature	55 °C
Operating current density	0.5 A cm^{-2}
Cell voltage (simulation/experiment)	0.64 V/0.658 V
Base case purge conditions	
Purge gas	N_2
Flow configuration	Co-flow
Cell temperature	55 °C
Inlet RH	0.4
Flow rate	3.74×10^{-6} m^3 s^{-1} (4.48 l min^{-1} for a 25 cm^2 cell with 24 channel parallel flow field design)

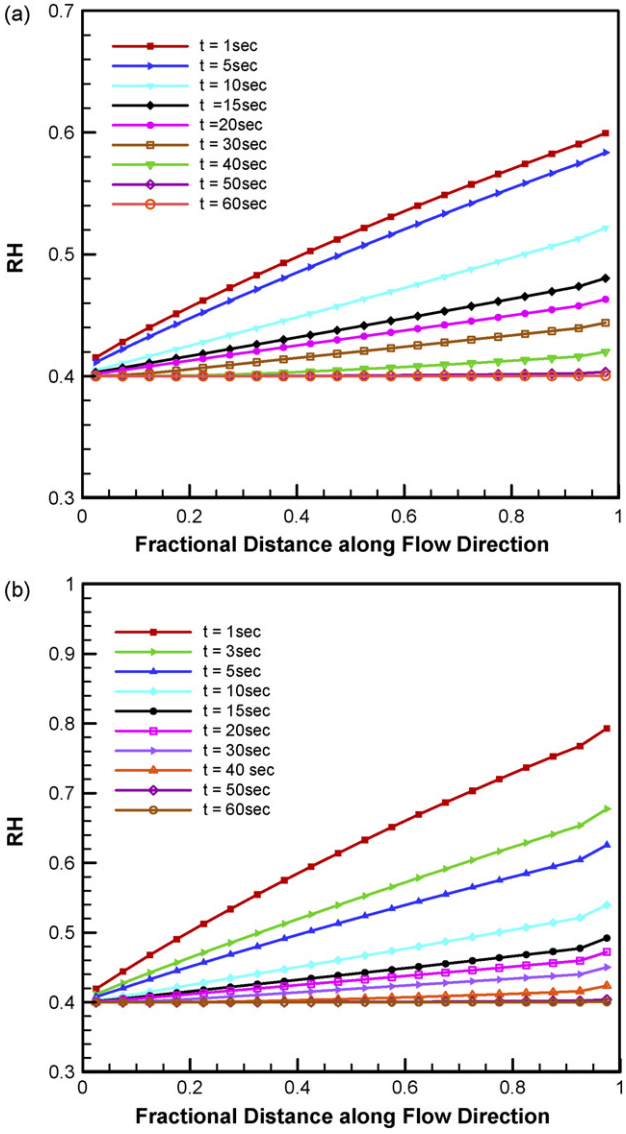

Fig. 2. RH variation in (a) anode gas channel and (b) cathode gas channel along the flow direction for gas purge with 40% inlet RH, 4.48 l min^{-1} flow rate and 55 °C cell temperature.

on the right-hand side of water conservation equation, will go to zero in the two-phase region whereas, the capillary flux term will diminish in the gas phase region. In addition, there exists ionomer or membrane phase in the catalyst layer. Therefore, the transient term for water conservation equation in CL should incorporate the removal of water content from ionomer phase, liquid and vapor phase from catalyst layer pores. The removal of water from electrolyte phase as well as CL pores is described through the effective factor, ε^{eff}, in the species equation listed in Table 1:

$$\varepsilon^{\text{eff}} = \varepsilon_{\text{g}} + \varepsilon_{\text{m}} \frac{\mathrm{d}C_{\text{w}}^{\text{m}}}{\mathrm{d}C_{\text{w}}} = \varepsilon_{\text{g}} + \varepsilon_{\text{m}} \frac{\rho_{\text{m}}}{\text{EW}} \frac{RT}{p^{\text{sat}}} \frac{\mathrm{d}\lambda}{\mathrm{d}a} \tag{16}$$

where ρ_{m} is the density of a dry membrane, EW the equivalent weight of membrane, ε_{m} the membrane phase water content and C_{w}^{m} the membrane phase water concentration. Note that the species equation in Table 1, encompasses the water transport equation in the anode and cathode catalyst layers, GDLs, and gas channels. In the membrane water content, λ, is solved from:

$$\frac{\partial \lambda}{\partial t} = \nabla \cdot (D_{\text{w}}^{\text{m}} \lambda) \tag{17}$$

where D_{w}^{m} is membrane water diffusivity. D_{w}^{m} is correlated to membrane water content, λ, which in turn depends on membrane water activity, a. In the present work, Gore-Select® membrane is used, whose properties are listed in Table 2. In gas purge the hydration of a membrane is measured by membrane HFR which can be determined from the membrane proton conductivity, κ. Using resistance network analogy, the cross-sectional average membrane HFR can be easily derived as

$$\frac{w_{\text{cell}}}{\text{HFR}} = \int_0^{w_{\text{cell}}} \frac{1}{\int_0^{\delta_{\text{mem}}} \mathrm{d}x/\kappa(\lambda)} \mathrm{d}y \tag{18}$$

The contact resistance is also accounted for to compute the cell HFR in accordance with experiments.

2.1. Boundary and initial conditions

The above-described equations are solved for five unknowns: $\vec{u}$ (three components), P and m_{w} (or λ in the membrane). Velocity at the gas channel inlet is specified as:

$$u_{\text{inlet}} = \frac{Q}{A_{\text{channel}}} \tag{19}$$

where Q and A_{channel} denotes purge gas flow rate and channel cross-sectional area. The inlet mass fractions are determined by the inlet pressure and relative humidity according to ideal gas law. Since gas purge is performed prior to engine shutdown, initial water distribution in PEFC is imported from a steady-state simulation of PEFC operation. More details of steady-state operation of PEFC can be obtained from Luo et al. [26].

2.2. Numerical implementation

The governing equations, summarized in Table 1, along with their appropriate boundary conditions are discretized by the finite volume method and solved in a commercial flow solver, STAR-CD®, by PISO algorithm (the pressure implicit splitting of operators), using its user defined capabilities. PISO is based on predictor–corrector splitting for unsteady problems. A constant time step size of 0.01 s is used in all simulations. In the present work, a single straight-channel PEFC with co-flow configuration, as depicted in Fig. 1, is considered. Based on the mesh independent study of Meng and Wang [30], the computational domain is discretized in approximately 34,000 computational cells, with 20 cells along the flow direction.

3. Results and discussion

The main geometric parameters and transport properties used in the present work are summarized in Table 3. Since gas purge

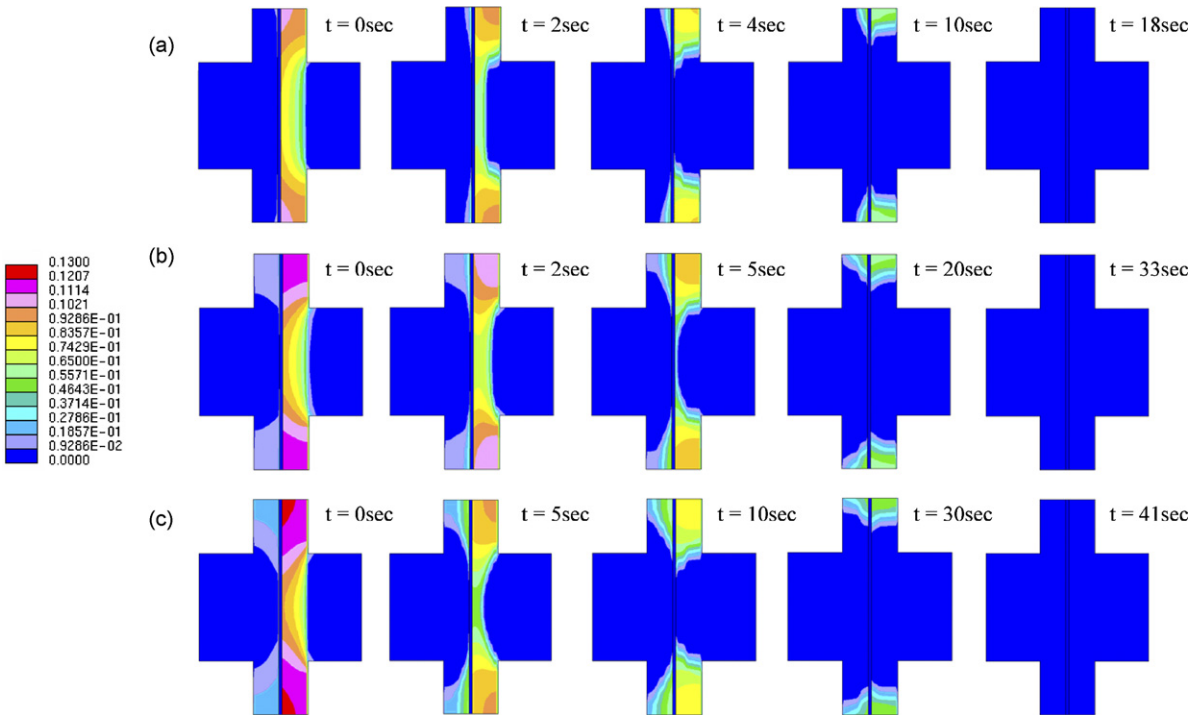

Fig. 3. Liquid saturation distribution as function of time at (a) inlet, (b) middle, and (c) outlet location along the flow direction for gas purge with 40% inlet RH, 4.48 l min^{-1} flow rate and 55 °C cell temperature.

is performed prior to engine shutdown, water distribution inside PEFC during pre-purge operation represents the initial condition for gas purge process. A pre-purge operation with operating conditions enlisted in Table 4 is simulated on the numerical mesh to obtain a realistic water distribution. The predicted cell voltage is found to be in good agreement with experimental data, as shown in Table 4. The purge conditions used in the present work are also mentioned in Table 4, and will be regarded as base case parameters in the following discussion. The gas flow rate mentioned in Table 4 is equivalent to 4.48 l min^{-1} flow rate in a fuel cell with 25 cm^2 active area and parallel flow field, assuming that flow is distributed uniformly in each channel. In the following, the flow rate will always be referred to that in the 25 cm^2 fuel cell.

Fig. 2 shows the RH variation along the flow direction in anode and cathode gas channels with purge time. Water mass flux into channel is inversely proportional to the distance of drying front away from the GDL-channel interface; therefore RH shoots to a very high value as purge starts. Less initial liquid saturation at the anode side results in less increase in RH along the anode gas channel in comparison to that in cathode gas channel. As the drying front proceeds further into porous layers, i.e. GDL and catalyst CL, RH in gas channel decreases with purge time as shown in Fig. 2. Additionally, due to water uptake RH increases monotonically along the flow direction. Fig. 3 displays the liquid water saturation as a function of purge time at three representative locations along the flow direction. At any location, the drying front first predominantly moves under the channel due to difficulty in water removal under the land portion. Once all the water under the channel portion is removed, drying front moves in the in-plane direction. The observed through-plane drying followed by in-plane drying stages is typical for gas purge. As can be seen, the drying time constant increases along the flow direction due to water uptake in gas channels entailing a total drying time of 18 s at the inlet section whereas 41 s at the outlet section. It should be mentioned that the variation of drying time along the flow direction is strongly dependent on purge gas flow rate. Investigations show that purge gas flow rate of 1.0 l min^{-1}, while keeping rest of the parameters the same, provides outlet drying time constant of 58 s. At low flow rate, channel RH increase along the flow direction due to water uptake is aggravated incurring substantially higher drying time towards the outlet section.

Variation of liquid water saturation with purge time in anode side is substantially different from that of in cathode side, highlighting the role of back diffusion from cathode to anode during gas purge. During pre-purge operation, cathode liquid water saturation is higher due to water generation. As purge starts, cathode liquid water saturation decreases due to water removal by evaporation and back diffusion through the membrane to the anode. Whereas on the anode liquid water saturation varies due to water removal by evaporation and water addition by back diffusion. The combined effect of back diffusion from cathode to anode and water removal by purge gas can be clearly seen in Fig. 4. Fig. 4 depicts the variation of average liquid water saturation as a function of purge time at three representative locations along the flow directions both in anode and cathode. In Fig. 4 at any location along the flow direction, purge time is non-dimensionalized with the total drying time constant at that location. In the beginning the average liquid water saturation in anode, as shown in Fig. 4(a), decreases with purge time. However, as purge time increases average liquid water saturation in anode increases due to back diffusion from cathode. Higher initial cathode liquid water saturation towards outlet section entails larger back diffusion and thereby larger increase in average anode liquid water saturation along the flow direction. As drying proceeds decrease in cathode liquid water saturation weakens back diffusion to anode that makes water removal by purge gas

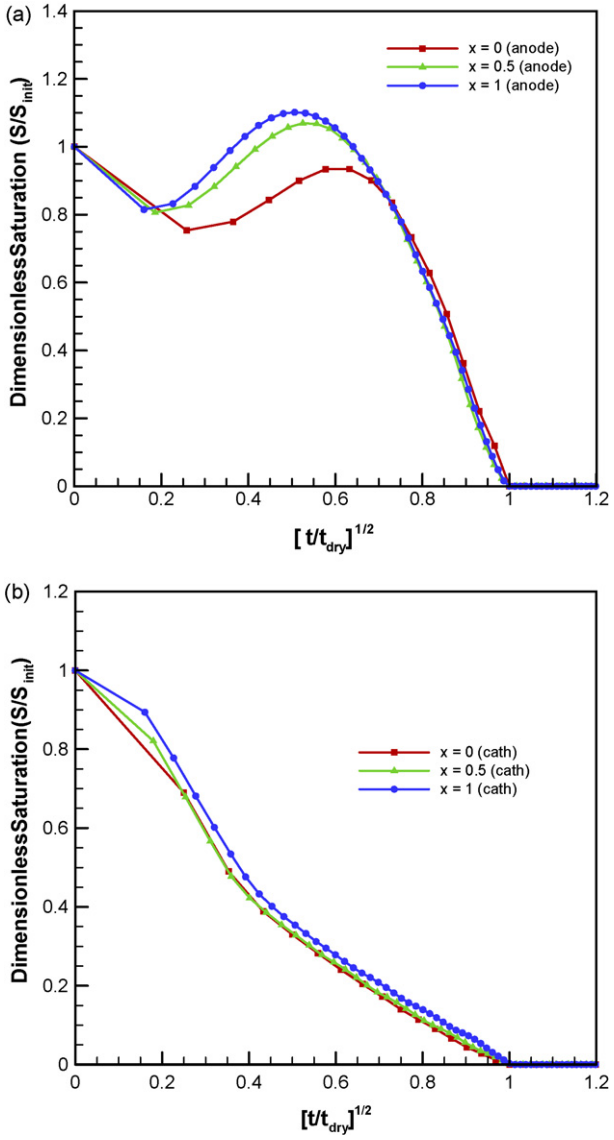

Fig. 4. Variation of average liquid water saturation along the flow direction in (a) anode and (b) cathode as a function of purge time for 40% inlet RH, 4.48 l min^{-1} flow rate and 55 °C cell temperature.

a dominant factor, resulting in monotonic decreases in anode liquid water saturation. The effect of back diffusion from cathode to anode becomes more pronounced at lower purge gas flow rates. Fig. 5 displays the variation of average liquid water saturation as a function of purge time when gas purge is conducted with 1.0 l min^{-1} flow rate while keeping rest of the parameters same as before. Smaller gas flow rate decreases the water removal rate from the channel and thereby renders a larger increase in RH along the flow direction. Higher RH in gas channel diminishes the water removal capacity by gas purge increasing the relative contribution of back diffusion from cathode to anode increases substantially, as seen in Fig. 5, especially towards the outlet of gas channel.

Due to sandwiched structure of PEFC, membrane drying is largely dependent on the evolution of the drying front in GDL. Therefore, GDL drying first in through-plane followed by in-plane drying incurs significant in-plane variation in the membrane water content. To clearly demonstrate the in-plane variation, average water content across the MEA under the channel and land portion is plotted in Fig. 6(a) and (b), respectively. The simulations

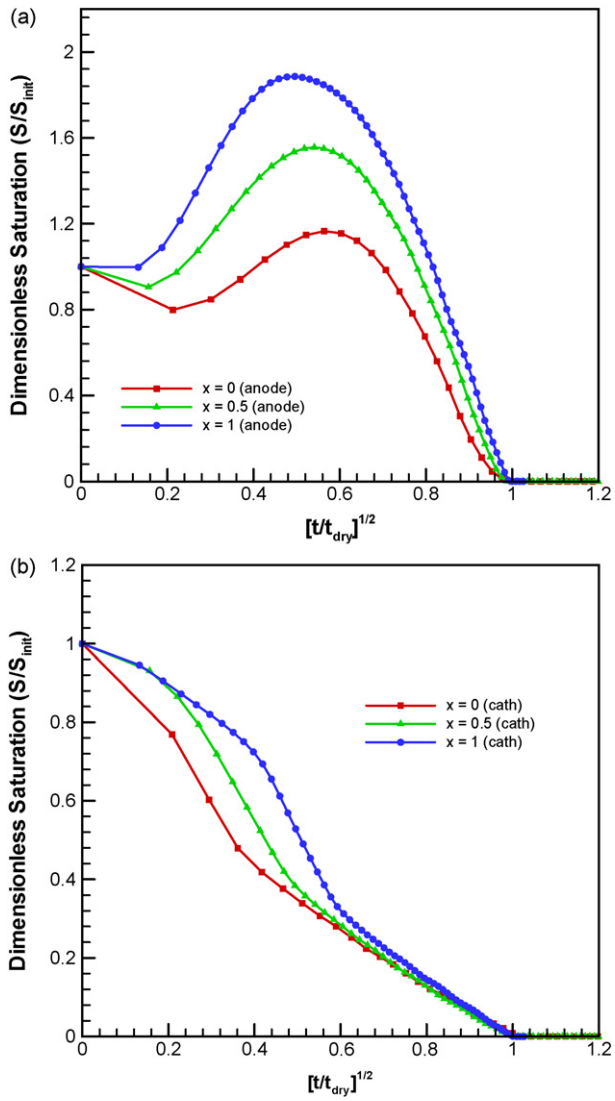

Fig. 5. Variation of average liquid water saturation along the flow direction in (a) anode and (b) cathode as a function of purge time for 40% inlet RH, 1.0 l min^{-1} flow rate and 55 °C cell temperature.

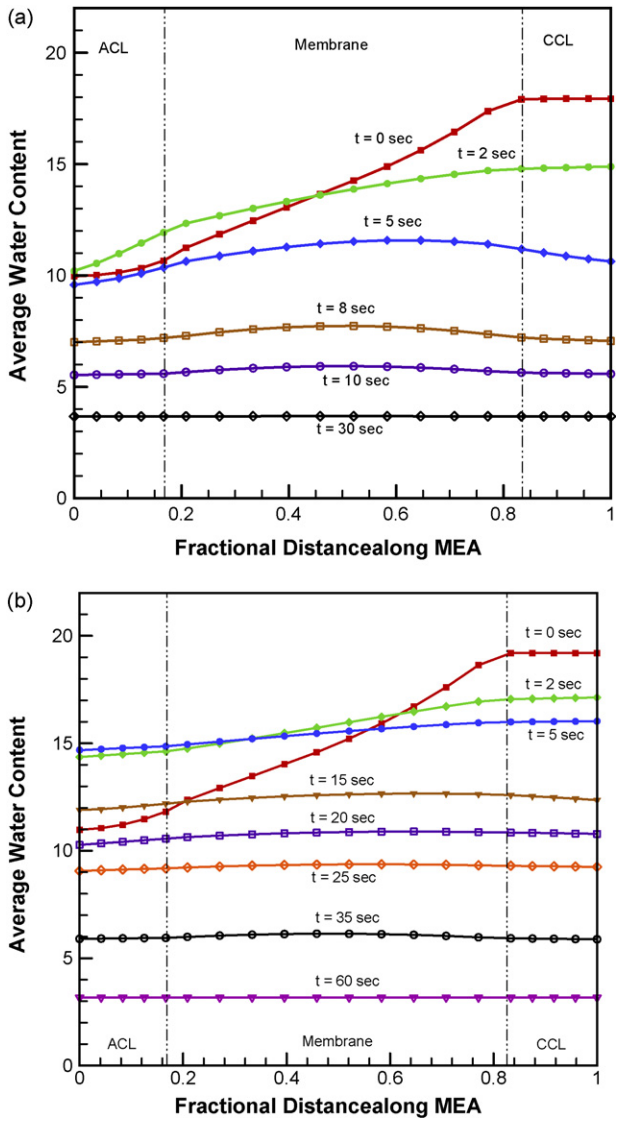

Fig. 6. Variation of average water content at a middle cross-section along the flow direction across MEA (a) facing channel and (b) facing land portion as function of purge time for 40% inlet RH, 4.48 l min^{-1} flow rate and 55 °C cell temperature.

are conducted with the base case purge conditions. For simplicity of analysis, water content is plotted at a middle cross-section along the flow direction. Initially water content is higher in cathode due to water generation during pre-purge operation. With the inception of purge, variation of the water content in the catalyst layers is governed by water removal by purge gas and back diffusion from cathode catalyst layer (CCL) to anode catalyst layer (ACL). At $t = 2$ s, a small increase in the water content of channel-facing ACL due to back diffusion can be seen in Fig. 6(a). In contrast, increase in water content of land-facing ACL is substantially higher, as shown in Fig. 6(b), owing to substantially slower water removal rate under the land portion. With further increase in purge time, MEA water content decreases and consequently diminishes back diffusion from CCL to ACL. It can be clearly seen in Fig. 6(a) that under the present conditions channel-facing membrane dries out at a very fast rate for first 10 s of purge whereas very little decrease in membrane water content is observed for $10\,\text{s} < t < 50\,\text{s}$, and can be attributed to decrease in water concentration gradient across GDL with time. The above-described variation of MEA water content with purge time become more pronounced at low purge gas flow rates. Fig. 7(a) and (b) displays variation of average water content across the MEA facing channel and land portion, respectively when purge is simulated with 1.0 l min^{-1} flow rate keeping rest of the parameters same. Low purge gas flow rate incur larger increase in RH in gas channels along the flow direction decreasing water removal capacity from PEFC. Therefore, the relative contribution of back diffusion from cathode to anode becomes more significant in membrane drying at low flow rates, as shown in Fig. 7(a) and (b). It should be mentioned that the minimum value of membrane water content is governed by the RH in gas channels entailing the minimum membrane water content of three corresponding to channel RH value of 40%, as displayed in Figs. 6 and 7.

Movement of drying front in PEFC is governed by vapor diffusion ahead of the drying front and liquid water transport due to capillarity from deep inside GDL to the drying front. The relative magnitudes of the two mechanisms determine the drying rate, and hence purge effectiveness. To evaluate the effect of capillary liquid water transport on purge, a parametric study is conducted by varying the contact angle in GDL and CL from 110° to 92° while keeping the rest parameters the same. A decrease in contact angle from 110° to 92° provides 10-fold decrease in liquid water transport

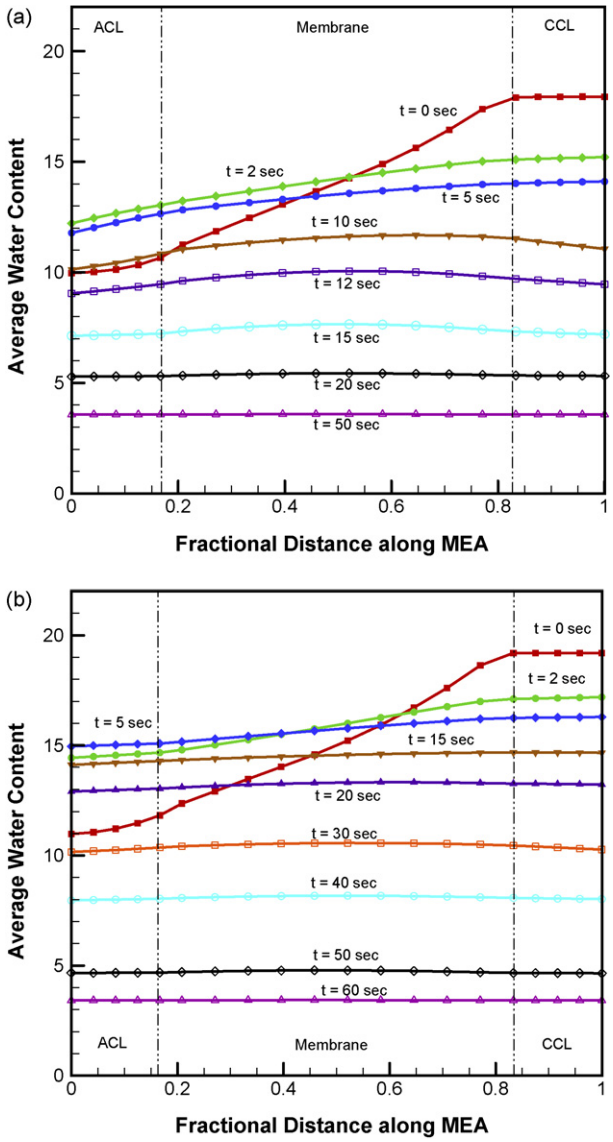

Fig. 7. Variation of average water content at a middle cross-section along the flow direction across MEA (a) facing channel and (b) facing land portion as function of purge time for 40% inlet RH, 1.0 l min^{-1} flow rate and 55 °C cell temperature.

behind the drying front. Fig. 8 shows the ensuing variation of membrane HFR with purge time for the two cases. Minimal difference in membrane HFR evolution with purge time as observed in Fig. 8 even when the contribution of liquid water transport differs 10 times for the two cases suggests that gas purge is mainly governed by evaporation and vapor diffusion ahead of the drying front. Therefore, it can be further concluded that tailoring various material properties and purge conditions rendering enhanced vapor diffusion will be most effective to improve gas purge effectiveness.

It is imperative to compare the predictions of the present gas purge model with experiments. Great effort has been made to carry out validation experiments and to ensure the reproducibility of purge data. Details of theses experiments can be found in Tajiri et al. [21]. Fig. 9 plots the predicted and experimentally measured membrane HFR variation with purge time under various purge conditions. As can be seen, a good match with experiments is obtained for 75.5 °C cell temperature whereas substantial differences exist in the shape of HFR profile for 55 °C cell temperature. The largest disparity between the predicted and experimentally measured pro-

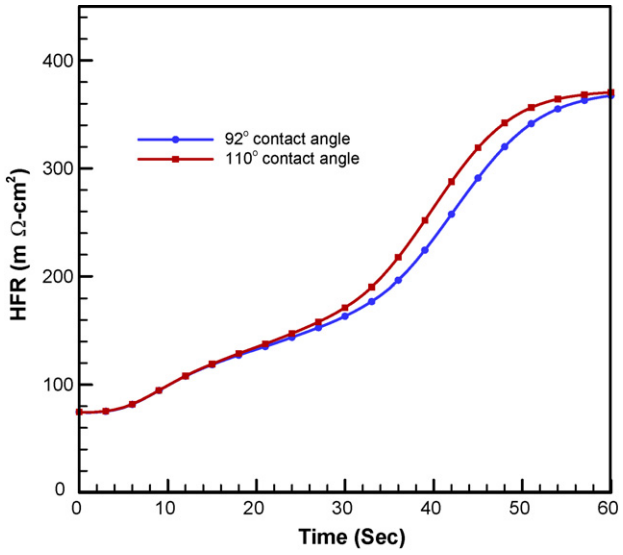

Fig. 8. Variation of membrane HFR with time as a function of contact angle.

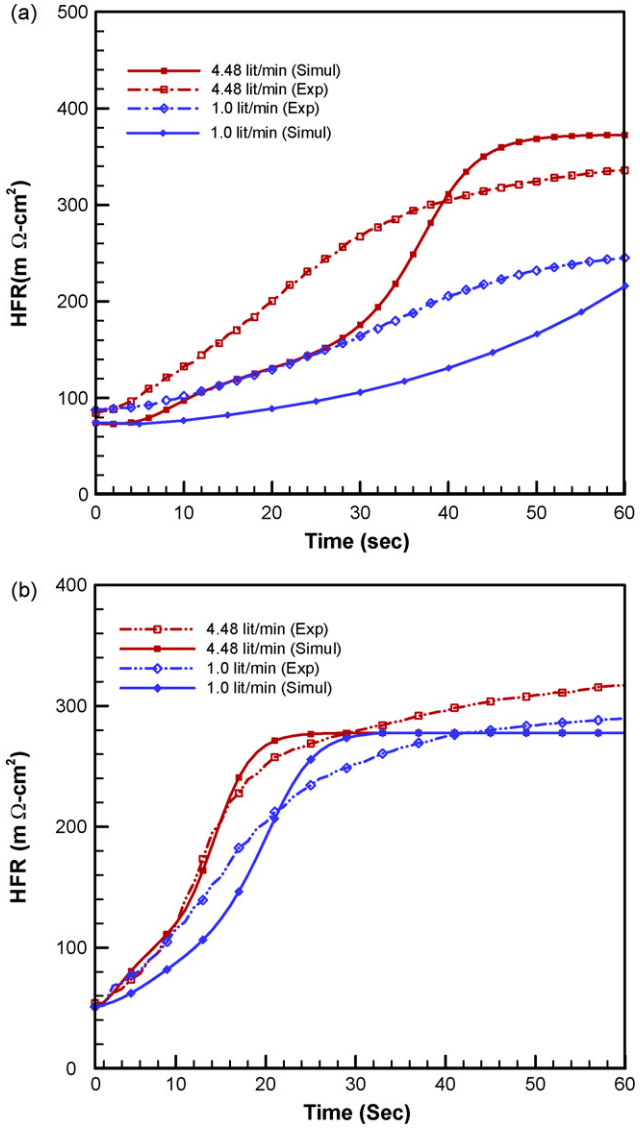

Fig. 9. Variation of membrane HFR with time for (a) 55 °C cell temperature and (b) 75.5 °C. Experimental variation is shown by dotted lines.

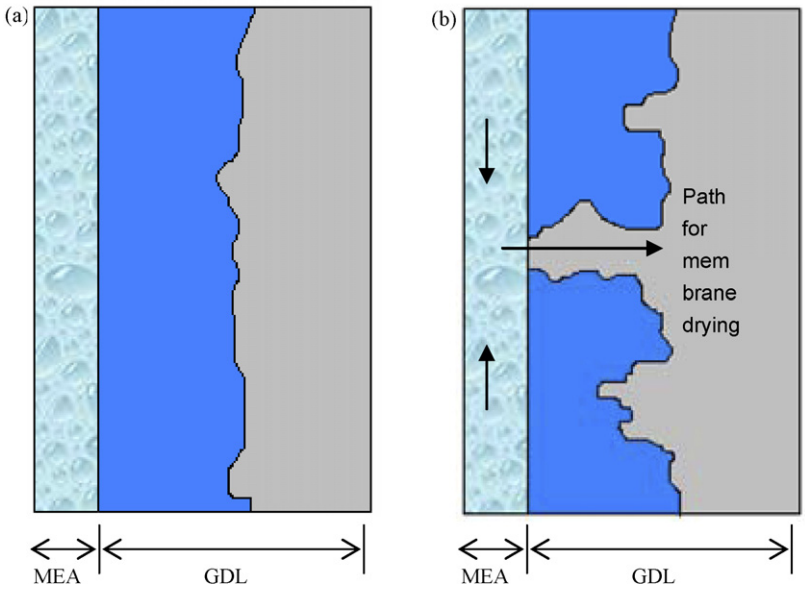

Fig. 10. Schematic representation of (a) compact drying front morphology and (b) finger-like morphology. Finger-like morphology provides path for membrane drying even before GDL completely dries out. Liquid water is shown by blue color. (For interpretation of the references to color in this figure legend, the reader is referred to the web version of the article.)

files is observed during the in-plane drying regime. This indicates that a more accurate description of liquid water distribution in GDL and CL is warranted during gas purge. The evolution of drying front morphology in PEFC can substantially affect membrane HFR profile, as shown schematically in Fig. 10. Fig. 10(a) depicts a compact morphology of drying front, inherently assumed in the present two-phase Darcy's law based macroscopic model, in which membrane cannot feel the effect of drying GDL dries out completely whereas, with finger-like morphology of drying front, as shown in Fig. 10(b), membrane can be dried out via deep fingers reaching membrane surface even before liquid water is completely removed from GDL rendering higher membrane HFR than compact morphology. Larger disparity between experimental and numerical results, as displayed in Fig. 9, can be due to the evolution of drying front with a compact morphology at high temperatures and with a finger-like morphology at lower temperatures. Therefore, a detailed understanding of the drying front morphology evolution in a realistic PEFC GDL is essential to address the observed differences in HFR profiles. Pore-level modeling efforts using a pore-network model [34] are currently underway to delineate the dependence of the drying front morphology on GDL microstructure, surface wettability, and purge conditions, and will be presented in a separate publication.

4. Conclusions

A fundamental understanding of gas purge mechanisms is essential to establish effective and energy-saving gas purge protocols. In the present work, a detailed two-phase transient purge model elucidating GDL and membrane drying is presented. It is found that under the realistic PEFC conditions, water removal is governed by capillary transport of liquid water from deep inside GDL to a drying front, vapor diffusion ahead of the drying front and water back diffusion through the membrane between the cathode and anode. Back diffusion assists water removal from the cathode but opposes water removal from the anode. The relative contribution of back diffusion in wetting the anode during gas purge is significant under the land portion and especially towards the outlet of gas channel. In the beginning of purge, water uptake in gas channel along the flow direction reduces water removal capacity of purge gas towards the outlet section enhancing the contribution of back diffusion in water removal. The investigations further conclude that cathode-only purge will not be effective as substantial amount of water can back diffuse to the anode and cannot be removed easily rendering a larger drying time constant.

The relative contribution of capillary transport of liquid water and vapor diffusion is also evaluated. A parametric study is conducted to investigate the effect of contact angle on HFR evolution. The results show that under realistic gas purge conditions, water removal from PEFC is largely governed by vapor diffusion ahead of the drying front. Therefore, it can be concluded that effective gas purge protocols can be established by engineering material properties or purge conditions that enhances water vapor diffusion in PEFC.

The model predictions are also compared with experimental results under various purge conditions. A good match with experiments is obtained at higher temperature whereas some differences in HFR profile shape is observed at lower purge temperature. The difference between numerical and experimental HFR profiles can be attributed to liquid water distribution especially during the in-plane drying regime. This warrants additional efforts to recognize various parameters controlling the evolution of drying front morphology in GDL as the drying front morphology can significantly affect membrane HFR.

Acknowledgements

Financial support for this work by Nissan Motor Co. Ltd. is gratefully acknowledged. The authors thank fruitful discussions with Y. Tabuchi.

References

[1] M. Oszcipok, D. Riemann, U. Kronenwett, M. Kreideweis, M. Zedda, J. Power Sources 145 (2) (2005) 407–415.
[2] L. Mao, C.Y. Wang, J. Electrochem. Soc. 154 (2007) B139–B146.
[3] L. Mao, C.Y. Wang, Y. Tabuchi, J. Electrochem. Soc. 154 (2007) B341–B351.
[4] K. Tajiri, Y. Tabuchi, C.Y. Wang, J. Electrochem. Soc. 154 (2007) B147–B152.
[5] S. Ge, C.Y. Wang, Electrochem. Solid-State Lett. 9 (2006) A499–A503.

[6] S. Ge, C.Y. Wang, Electrochim. Acta 52 (2007) 4825–4835.
[7] A.V. Luikov, Int. J. Heat Mass Transf. 18 (1975) 1–14.
[8] S. Whitaker, Adv. Heat Transf. 13 (1977) 119–203.
[9] O.A. Plumb, G.A. Spolek, B.A. Olmstead, Int. J. Heat Mass Transf. 28 (1985) 1669–1678.
[10] M. Ilic, I.W. Turner, Appl. Math. Model. 10 (1986) 16–24.
[11] M. Ilic, I.W. Turner, Int. J. Heat Mass Transf. 32 (1989) 2351–2362.
[12] S.B. Nasrallah, P. Perre, Int. J. Heat Mass Transf. 31 (1988) 957–967.
[13] M. Quintard, S. Whitaker, Adv. Heat Transf. 28 (1993) 369–464.
[14] J.A. Rogers, M. Kaviany, Int. J. Heat Mass Transf. 35 (1992) 469–480.
[15] S. Whitaker, W.T.H. Chou, Drying Technol. 1 (1) (1983) 3–33.
[16] M. Kaviany, M. Mittal, Int. J. Heat Mass Transf. 30 (1987) 1407–1418.
[17] C.L.D. Huang, Int. J. Heat Mass Transf. 22 (1979) 1295–1307.
[18] M.G. Goyeneche, D. Lasseux, D. Bruneau, Trans. Porous Media 48 (2002) 125–158.
[19] T. Lu, P. Jiang, S. Shen, Heat Mass Transf. 41 (2005) 1103–1111.
[20] N. Shahidzadeh-Bonn, A. Azouni, P. Coussot, J. Phys.: Condens. Matter 19 (2007) 112101–112107.
[21] K. Tajiri, C.Y. Wang, Y. Tabuchi, Electrochim. Acta 53 (2008) 6337–6343.
[22] R. Bradean, H. Haas, A. Desousa, R. Rahmani, K. Fong, K. Eggen, D. Ayotte, A. Roett, A. Huang, Proceedings of the AIChE 2005 Annual Meeting, Cincinnati, OH, October 30–November 4, 2005.
[23] P.K. Sinha, P. Halleck, C.Y. Wang, Electrochem. Solid-State Lett. 9 (2006) A344–A348.
[24] P.K. Sinha, C.Y. Wang, J. Electrochem. Soc. 154 (2007) B1158–B1166.
[25] Y. Wang, C.Y. Wang, J. Electrochem. Soc. 154 (2007) B636–B643.
[26] G. Luo, H. Ju, C.Y. Wang, J. Electrochem. Soc. 154 (2007) B316–B321.
[27] C.Y. Wang, P. Cheng, Int. J. Heat Mass Transf. 39 (1996) 3607–3618.
[28] U. Pasaogullari, C.Y. Wang, J. Electrochem. Soc. 151 (2004) A399–A406.
[29] R.B. Bird, W.E. Stewart, E.N. Lightfoot, Transport Phenomena, John Wiley & Sons, New York, 1960.
[30] H. Meng, C.Y. Wang, Chem. Eng. Sci. 59 (2004) A3331–A3343.
[31] H. Ju, C.Y. Wang, S. Cleghorn, U. Beuscher, J. Electrochem. Soc. 152 (2005) A1645–A1653.
[32] K. Tajiri, Private communications (2006).
[33] U. Pasaogullari, C.Y. Wang, J. Electrochem. Soc. 152 (2005) A380–A390.
[34] P.K. Sinha, C.Y. Wang, Electrochim. Acta 52 (2007) 7936–7945.